STRAIN GAUGE VALIDATION OF FINITE ELEMENT ANALYSIS OF A TI6AL4V (ELI) MANDIBULAR IMPLANT PRODUCED THROUGH ADDITIVE MANUFACTURING

L.F. Monaheng [1*], W.B. Du Preez[2] & A. Olwagen[3], P. Haupt[4]

[1,2]Department of Mechanical and Mechatronics Engineering
Central University of Technology, Free State
[1]lmonaheng@cut.ac.za
[2]wdupreez@cut.ac.za

[3]Private consultant
olwagen.lienie@gmail.com

[4]National Aerospace Centre, University of the Witwatersrand
Philip.Haupt@wits.ac.za

ABSTRACT

Medical implants created by Ti6Al4V (ELI) through Additive Manufacturing (AM) processes have a very positive impact on the quality of life of patients who have undergone bone reconstructive surgery. The effectiveness of medical implant design for AM processes would be significantly improved if finite element analysis (FEA) could be established as an accepted design tool. This study is aimed at validating FEA as a tool for predicting the strain distribution in a Ti6Al4V (ELI) medical implant produced through a selective laser melting (SLM) process by comparing the FEA results with strain gauge measurements.

The approach followed was to demonstrate the correlation between an FEA model and strain gauge measurements performed on a human mandibular implant. For the design of the mandibular implant the geometrical representation of an adult human mandible obtained from a computerized tomography (CT) scan was used. This CAD model was then submitted to FEA when subjected to typical static mastication load conditions. Through this simulation the distribution of strain in the implant was determined. Using the same CAD model, an implant was manufactured through SLM and strain gauges were mounted on the implant at locations corresponding to the areas of highest strain as determined on the FEA model.

The results obtained from both FEA and strain gauge measurements are presented in this paper, and a correlation within an error margin of less than 10 % for most of the gauge was obtained. Requirements for achieving this level of correlation are discussed. It is concluded that FEA is indeed a powerful tool for improving the effectiveness of design for AM of medical implants.

*Corresponding author

1. INTRODUCTION:

According to the ASTM F2792 standard, Additive Manufacturing (AM) is defined as, "the process of joining materials to make objects from three-dimensional (3D) model data, usually layer upon layer, as opposed to subtractive manufacturing technology"[1]. This technology is applied through various processes, such as Stereo-lithography (SL), Fused Deposition Modelling (FDM), Selective Laser Sintering (SLS) and 3D printing [2]. Currently, AM processes are divided into seven categories which include Vat Photo-polymerization, Material Jetting, Binder Jetting, Material Extrusion, Sheet Laminating, Direct Energy Deposition and Powder Bed Fusion [1].

AM technology has been applied very successfully for the production of medical implants [3][4]. However, in order to produce a sound design, it is imperative to understand the strain distribution and resultant deformation that such an implant will experience once implanted in the patient's body. It has been found that an implant fails due to occlusal overloading [5] and other factors such as impact [6] [7]. It is through that the effectiveness of the process of designing medical implants for AM could be improved, provided that finite element analysis (FEA) be established as a reliable design tool for design of AM medical implants.

FEA is widely accepted as a powerful modelling tool in many areas of science and engineering [8]. It has also been used in the medical field to predict the behaviour of complex structures, such as mandibular implants [9] [10]. Nevertheless, to establish confidence in the results of an FEA model, some form of experimental verification is required. There two techniques that are used to validate FEA models, namely strain gauge and optical sensor techniques [11] [12][13]. Strain gauges could provide an accurate validation of FEA, provided that the selected positions of the gauges on the surface of the computationally analysed model correspond accurately with those on the experimental model.

This paper presents the approach taken and the results obtained to validate FEA as a reliable tool for predicting the strain distribution in a Ti6Al4V (ELI) mandibular implant produced through AM.

2. RESEARCH PROCEDURE

2.1 Computational Analysis

2.1.1 Computer Aided Design

The design of a computer aided design (CAD) model suitable for computational analysis and experimental validation was based on a three dimensional mandibular implant model designed in SOLIDWORKS® that represents an adult human mandible. This mandibular CAD model was generated from computer topography (CT) scan data of a patient and was made available for this study by the Centre for Rapid Prototyping and Manufacturing (CRPM). In Figure 1 (a) and (c) this mandibular CAD model as produced through the CT data is shown. From this CAD model a mandible implant was designed and is shown in Figure 1 (b) and (d).

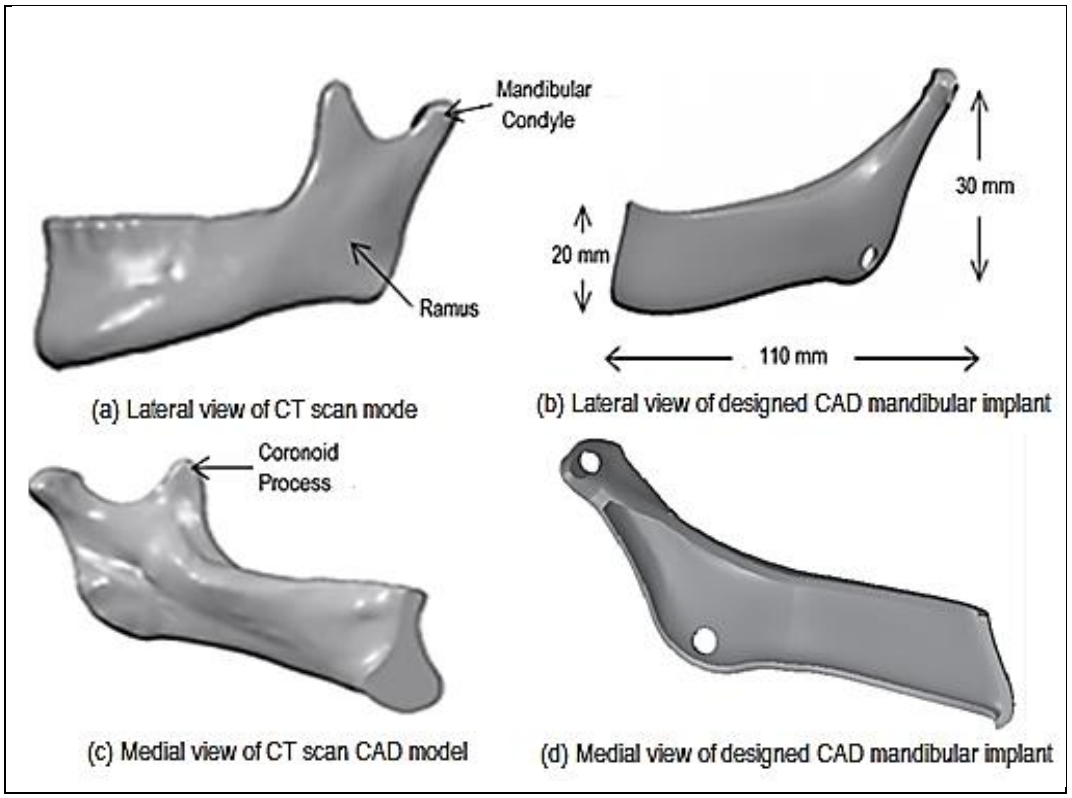

Figure 1: The different views of the mandibular CAD model obtained from CT scan data (a) and (c) provided as basis for the study and the designed mandibular implant CAD model (b) and (d).

The mandibular implant CAD model was designed in such a way that both internal and external surfaces of the mandibular implant would be as flat as possible to allow the proper installation of strain gauges. The mandibular condyle's dimension and shape on the designed implant was kept the same as the original CAD model because, if it was to be used on a patient, it should be able to articulate with the temporal articulation surface of that specific patient. However, the coronoid process was cut out on the implant since this appeared to be common practice when designing mandibular implants [14][15].

The elastic modulus (Young's modulus = E) of the titanium implants is different to that of the bone. This modulus difference causes an inefficient transfer of load from the implant to the bone. The subsequent stress shielding leads to bone resorption and eventual loosening of the implant [3]. However, through the effective geometrical design of the implant more effective transfer of the load between bone and titanium implant could be achieved. Therefore, the implant design was aimed at achieving less geometrical stiffness, while still maintaining sufficient strength to ensure that it would not fail when a typical mastication load is applied on it. Therefore, a safe wall thickness (t) of the mandibular implant model was found to be 2 mm. This wall thickness was determined by using the ratio of the modulus of elasticity of titanium as compared to bone and multiplying by a safety factor of 4 (see equation (1)).

$$t_{implant} = \frac{E_{bone} \cdot t_{bone}}{E_{implant}} (\text{safety factor}) \quad (1)$$

In this calculation the mandible cortical bone thickness (t_{bone}) was taken as 3.8 mm as specified in literature [16] [17].

A hole at the ramus of the mandibular implant was created to represent the position of the attachment of the masseter muscle. Besides that, another hole was created on the implant's condyle for fixing the mandibular implant during experimental loading.

2.1.2. Initial Finite Elements Analysis

The current study is based on a linear static analysis. Patran software was used for pre and post-processing whereas Nastran software was used as a solver. Firstly, the mandible implant CAD model was imported into the Patran software to create the quadratic tetrahedral (commonly known as Tet 10) solid mesh with a global element edge length of 2 mm. These meshes consist of a linear and quadratic shape function. Tet 10 (second complete-polynomial member) is significantly better for stress analysis in structures and solid mechanics such as medical implants. However, in the areas of strain gauge attachment the mesh was refined to enable more accurate comparison with the experimental measurements. To refine the mesh a uniform mesh seed was created around the gauge area to achieve a denser mesh. Secondly, the isotropic homogeneous material properties of Ti6Al4V (ELI) were assigned to the FEA model. Table 1 shows the titanium material properties which were applied.

Table 1: Titanium material properties [18].

Material Ratio	Elastic Modulus (GPa)	Shear Modulus (GPa)	Poisson's ratio	Density (kg/m^3)
Ti6Al4V (ELI)	110	40.74	0.35	4400

Once the material properties were assigned the load and boundary conditions were set up. The condyle of the mandible implant CAD model was fixed in such a way that it could rotate only about the axis perpendicular to the Z-Y plane which passes through point **A**. Besides that, the condyle was also restricted from translating in all directions. On the other side of the implant (point **B**) only one direction was restrained which is the translation in the Z direction (see Figure 2). Note that R_1 and R_2 are the reaction forces acting at the inner surface of the condyle's hole and the top surface of the implant at B, respectively. These boundary conditions were based on Koolstra's study on the human mastication system [19][20].

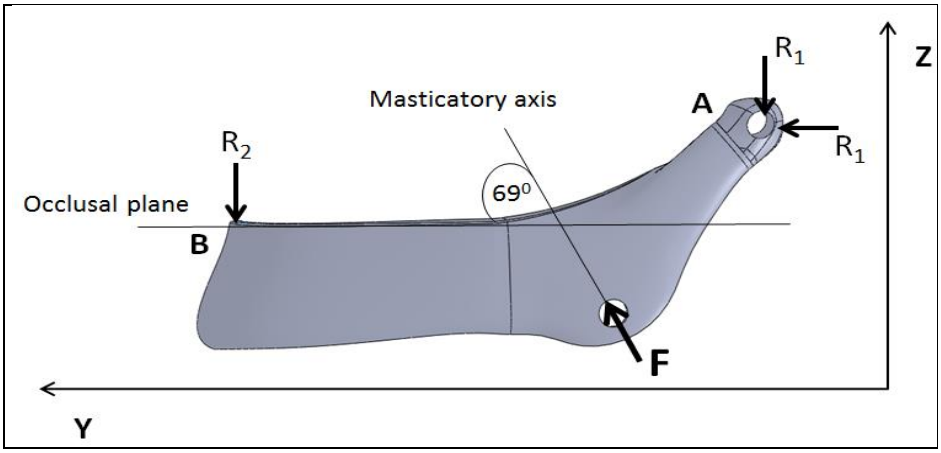

Figure 2: Experimental loading and boundary conditions of the mandibular implant. Where: R_1 and R_2 represent the reaction forces on the condyle and the front end of the implant, respectively, and F is the applied total load on top inner surface of the hole.

The maximum load of 1 025 N was applied on the top inner surface of the hole at an angle of 69^0 with regard to the occlusal plane, but parallel to the masticatory axis of the implant CAD model. This angle was set based on the fact that both the masseter muscle and the mastication axis remain approximately 69^0 with regard to the occlusal plane regardless of the inter-skeleton variations [21].

The implant was designed to withstand the maximum biting load. The maximum force a person with healthy teeth can apply when biting is 2 091 N [22] [23]. Therefore, the symmetrical half should withstand 1 046 N.

2.1.3. Determination of strain gauge positions

The Von Mises stress distribution found from the initial FEA was used to identify the possible positions where strain gauges could be installed. The strain gauges were installed on areas of highest stress where strain values could easily be detected by the gauges, but not close to the fixation points of the implant. Because the fixation points were points of localised stress concentration and could lead to misleading results, they were avoided. In Figure 3 (a) and (c) the FEA results used to determine the preferred strain gauge positions are indicated.

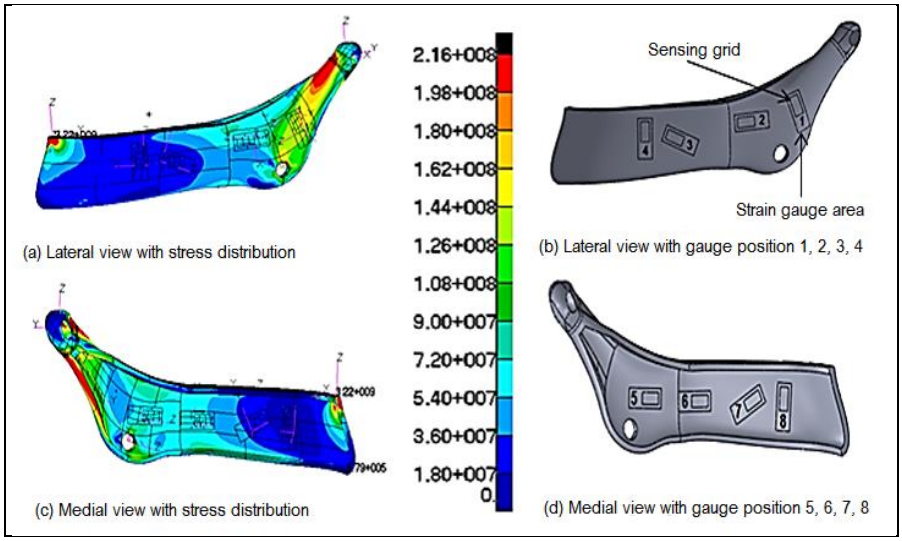

Figure 3: Von Mises Stress distribution profiles of the mandible implant CAD model (a) and (c) and the mandible implant CAD model (b) and (d) showing the selected gauge positions

The type of strain gauge used for experimental measurement of strain is shown in Figure 4.

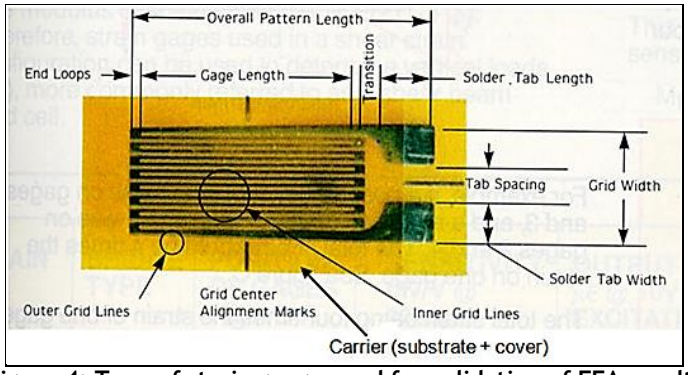

Figure 4: Type of strain gauge used for validation of FEA results

The directions to which the gauge lengths of the strain gauges should be aligned, were determined by plotting the marker vectors of the principal strain. It was decided that a strain gauge should be installed in the direction of the Z component of the principal strain vector to make sure that it

corresponds with the calculated strain. In Figure 5 the super positioned area of the strain gauge with the marker vector illustrating the direction of the principal strain, is shown.

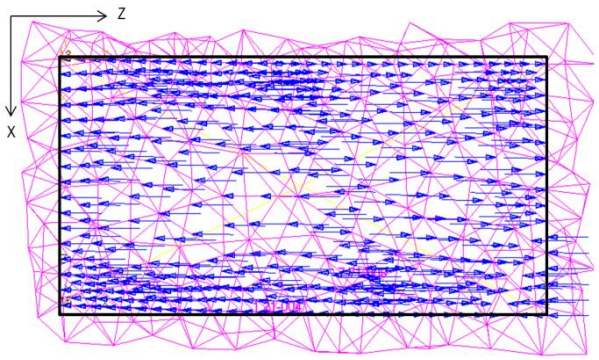

Figure 5: Superposition of the area of the strain gauge onto the FEA mesh to align with the direction of the principal strain.

The areas identified for strain gauges were marked on the CAD model used for producing the experimental implant. This assisted with the positioning and alignment of the strain gauges on the experimental model during the gauge installation. The dimensions of the whole gauge are 5 mm x 12 mm and that of the sensing grid are 3 mm x 8 mm. In order to simplify FEA interpretation, the CAD surfaces were split on the periphery of the strain gauges, such that the nodes corresponding to the gauge sensing areas could be grouped separately as shown in Figure 5. The orientations of the strain gauges on the implant CAD model shown in Figure 3 (b) and (d) were derived through this approach.

An additional advantage of the initial FEA was to confirm that the implant would not fail when the typical maximum load was applied. For this, the commonly used failure criteria of ductile materials (Von Mises failure criteria) were applied. According to these criteria, if the Von Mises stress calculated is greater than the yield stress of the material, failure occurs [24]. The maximum Von Mises stress found under the maximum loading conditions of 1 026 N applicable to the mandible implant was 216 MPa. This clearly indicated that the implant would not fail under maximum load, because the maximum stress generated on the implant due to the applied force was much less than the yield stress of the titanium material which is typically 930 MPa [25].

2.1.4. FEA on the mandibular implant CAD model

Finally, FEA was performed on the modified mandibular CAD model under different load magnitudes, to determine the corresponding strain distributions. Because the muscles of mastication exert variable forces on the mandible to provide the different biting pressures, it was decided to simulate reality by performing the FEA simulations with different loads. Five FEAs were performed with different loads namely, FEA: A = 215 N, FEA: B = 415 N, FEA: C = 620 N, FEA: D = 821 N and FEA: E = 1 026 N. For each load the mesh, boundary conditions and the material properties were kept constant. As expected, a direct relationship between the applied load and the principal strain was found. In Figure 6 (a) and (b) the obtained results are shown.

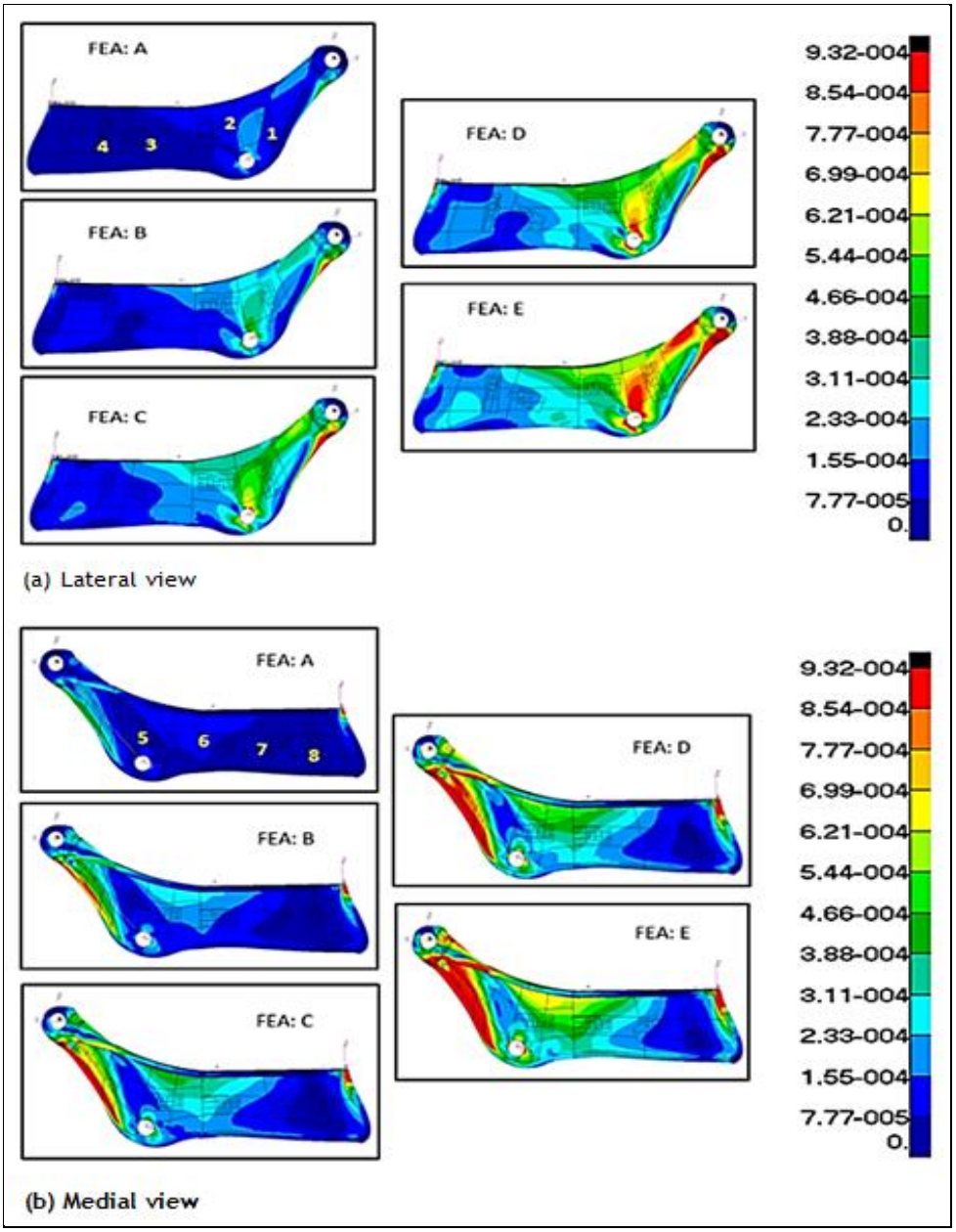

Figure 6: Lateral and medial view of the maximum principal strain distribution on the mandibular implant for different loadings. FEA: A = 215 N, FEA: B = 415 N, FEA: C = 620 N, FEA: D = 821 N and 1 026 N.

2.2. Experimental Analysis

2.2.1. Additive manufacturing

For the experimental analysis an additive manufacturing technology was used to manufacture the mandibular implant at the CRPM. An EOSINT M280 direct metal laser sintering (DMLS) machine was used to manufacture the implant. In this process Ti6Al4V powder was fused layer by layer to form the mandibular implant directly from the mandibular implant CAD model. In Figure 7 the experimental model or additively manufactured implant is shown.

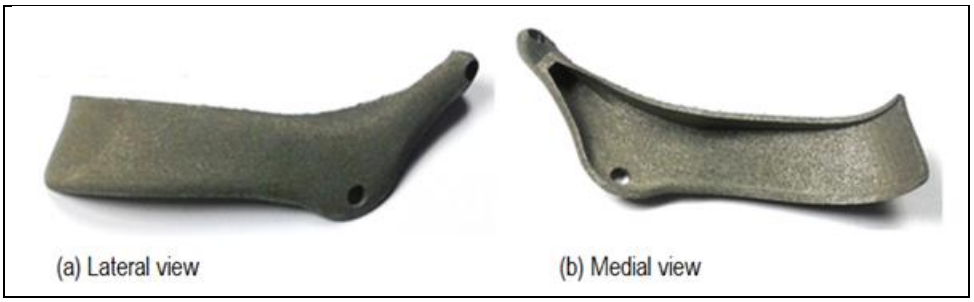

Figure 7: Additively manufactured Ti6Al4V mandibular implant

2.2.2. Heat treatment of the mandibular implant

During the SLM process residual stress is induced in the mandibular implant, which can affect its mechanical properties. Therefore, a stress relieving heat treatment was performed on the implant. During this treatment the implant was heated in a furnace under a protective argon atmosphere at a temperature ramp up rate of 200 ^{0}C per hour until it reached 650 ^{0}C. Subsequently, it was kept at this temperature for 3 hours and then allowed to slowly cool down in the furnace. Thereafter, a beta anneal treatment was performed on the implant under vacuum at the CSIR. In this process the implant was heated over a ramp up time of 4 hours to 950 ^{0}C and furnace cooled to room temperature to allow alpha grain growth, resulting in increased ductility of the alloy. Finally, the implant was heated to 950 ^{0}C, kept at temperature for a period of 2 hours and then furnace cooled over 4 hours.

2.2.3. Experimental procedure

To establish experimental loading and boundary conditions of the mandibular implant that would comply with those of the FEA discussed in 2.1.2 and indicated in Figure 2, the experimental test bench shown in Figure 6 was designed and manufactured. The test bench was designed and constructed to not deform as the load was applied. Its frame was made from mild steel with 15 mm X 15 mm X 2 mm square tubing reinforced by 3 mm thick plate at the top. The implant's condyle was connected by a 5 mm diameter mild steel pin in such a way that it forms a hinge about an axis perpendicular to the Z-Y plane and passes through point A as shown in Figure 8 (b). Moreover, the condyle was restricted from translation in all directions by the steel blocks. On the other side of the implant (point B or front end) only one direction was prohibited. The load cell was hooked between the implant and the load hanger to accurately measure the force applied on the mandibular implant. This load was experienced by the implant at the point where the pin was inserted through the implant to represent the attachment position of the masseter muscle.

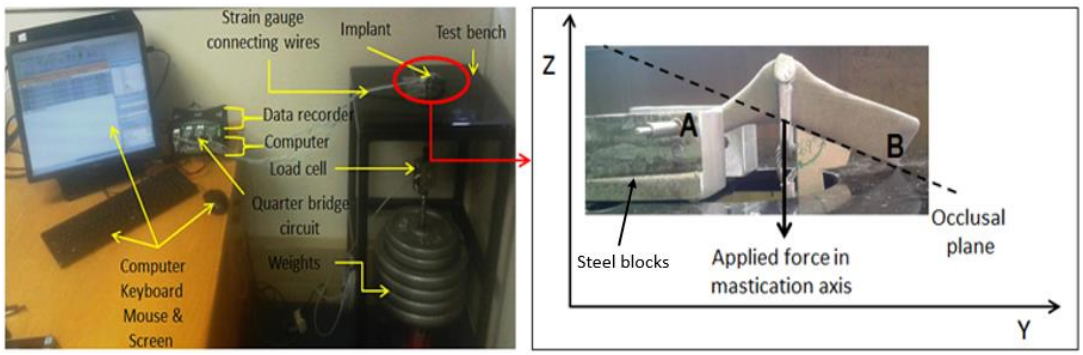

(a) Complete assembly (b) Load and boundary conditions

Figure 8: Experimental test bench used to achieve the load and boundary conditions.

In these experiments the 350±0.3% ohms type of strain gauge (6/350 LY41 student gauge) with a gauge factor of 2.03±1% as shown in Figure 4 were used. The strain gauges were installed on the implant and connected to a Wheatstone circuit known as a quarter bridge circuit (1-SCM-SG120) by a 3 wire configuration. Thereafter, each circuit was connected to the specific channel of the data recorder (Quantum X, CX 22W with 8 channels). Once the load was applied on the implant the strain values were recorded and delivered to the computer through Catman® software. In Figure 9 the experimental data collection system is shown.

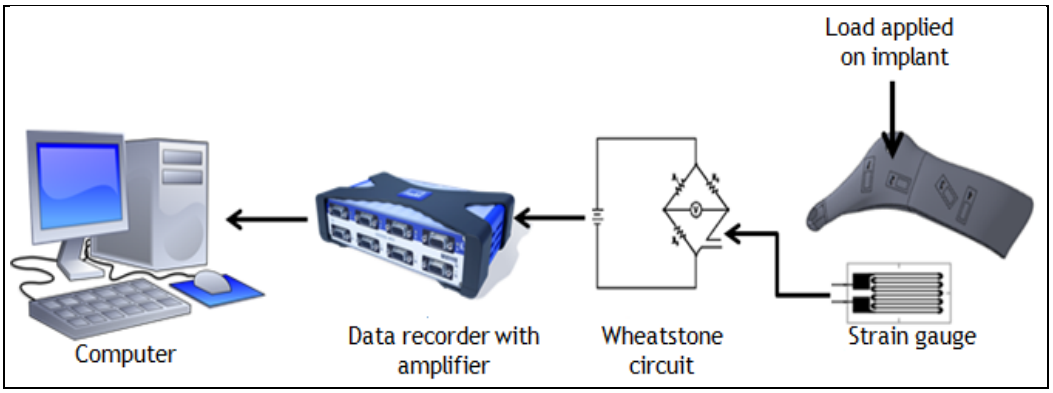

Figure 9: Strain gauge connection through Wheatstone bridge circuit to data recorder and computer

The system allowed data from a number of strain gauges to be collected simultaneously. The strain gauges were installed on the surfaces of the mandibular implant at the positions shown in Figure 3. On application of the load on the implant each gauge started to record the data at a frequency of 0.5 Hz. This implied that for a single test each gauge recorded 133 data samples over a period of 266 seconds. Each test was repeated three times to determine the repeatability of the measurements. In Figure 10 the repeatability of the all gauges are illustrated for Experiment A with a load of 215 N. Clearly, the initial part of the graph represents a transitional region when the it takes a few seconds to reach the stable region of strain. Only values obtained after 33 seconds were used.

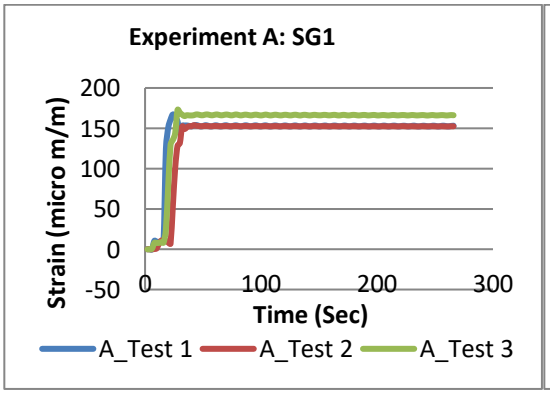

(a) Strain gauge 1

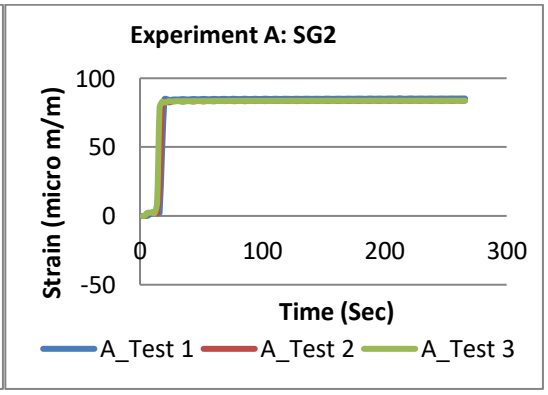

(b) Strain gauge 2

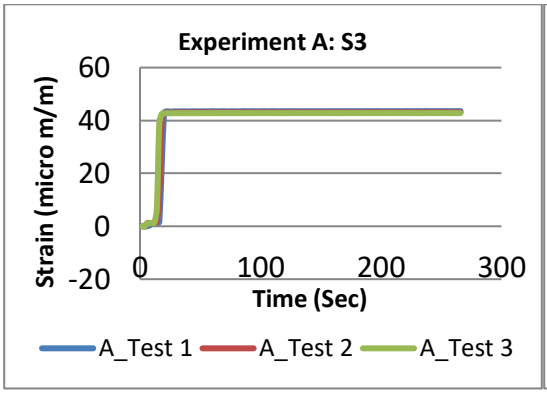

(c) Strain gauge 3

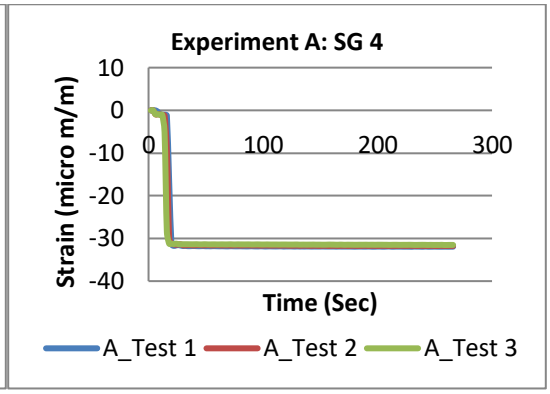

(d) Strain gauge 4

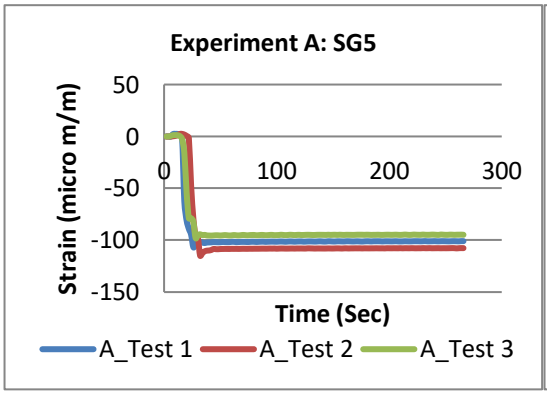

(e) Strain gauge 5

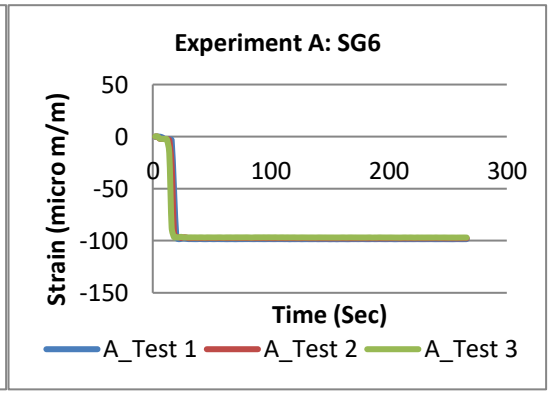

(f) Strain gauge 6

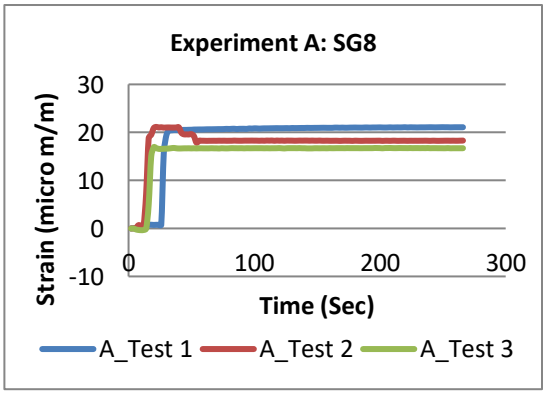

(g) Strain gauge 8

Figure 10: Graphical representation of strains against time for all strain gauges captured in first experiment A = 215 N.

During this experiment it was found that strain gauge 7 deviated drastically from the other gauges and was clearly not recording the strain correctly. It was, therefore, decided not to use data from this gauge in subsequent experiments.

To determine the effect of different loads and compare these with the FEA results, four more experiments were performed following the same process as in experiment A, namely experiment B

= 415 N, experiment C = 620 N, experiment D = 821 N and experiment E = 1 026 N. In each experiment only loads were changed and the boundary conditions were kept constant.

3. RESULTS AND DISCUSSIONS

The FEA strain values were compared with the experimental strain values for different loads for all the strain gauges. Figure 11 (a) to (g) illustrates the correlation between the FEA and the experimental values for different experiments as detected by the different strain gauges. Figure 11 clearly shows that there is a very good correlation between experimental and FEA results.

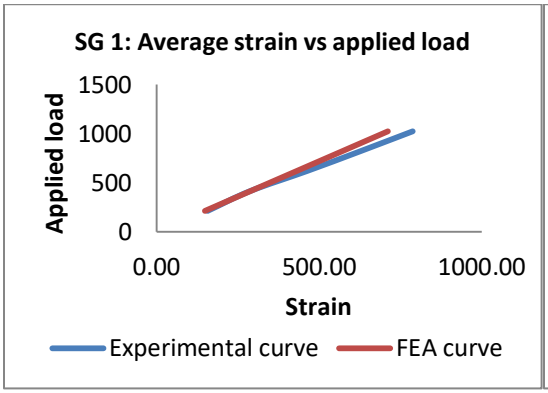

(a) Strain gauge 1

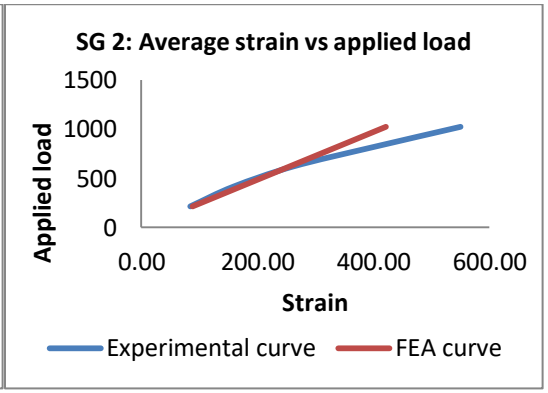

(b) strain gauge 2

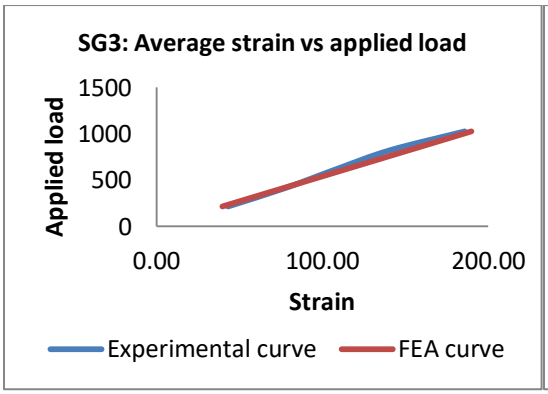

(c) Strain gauge 3

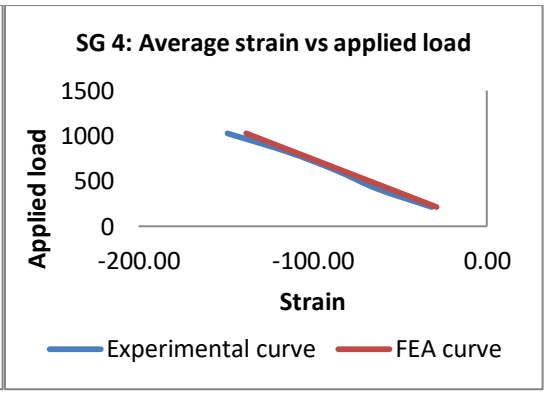

(d) Strain gauge 4

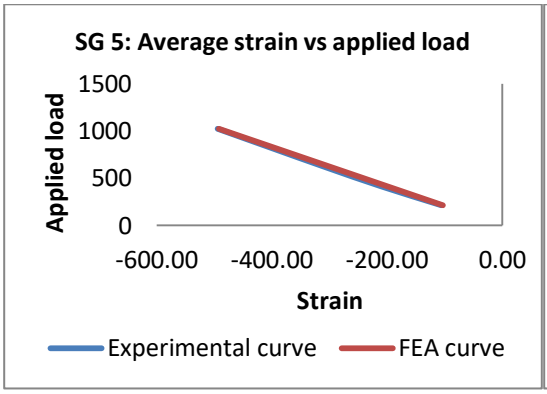

(e) Strain gauge 5

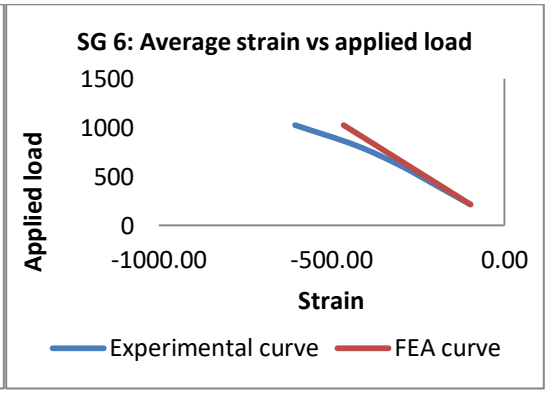

(f) Strain gauge 6

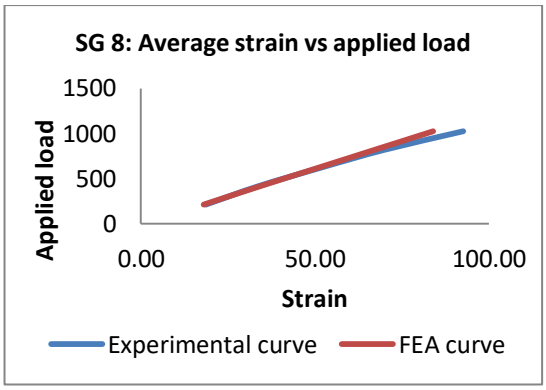

(g) Strain gauge 8

Figure 11: Comparison of the FEA results with the experimental results over the range of loads

The percentage deviation of the FEA results from the experimental results was calculated for each strain gauge using equation (2). In table 2 correlation between FEA and experimental results tabulated.

$$\text{Percentage of deviation} = \left(\frac{\text{Experimental strain value - FEA strain value}}{\text{Experimental strain value}}\right) 100 \qquad (2)$$

Table 2: Comparison of experimental results versus FEA strain results

	SG1	SG2	SG3	SG4	SG5	SG6	SG8	Load (N)
#Nodes	177	181	169	193	193	173	*177*	
Experiment A FEA_A *% deviation*	157.21 148.87 5.61	84.13 88.17 -4.58	43.13 39.70 8.65	-31.69 -28.94 9.52	-101.32 -102.92 -1.56	-97.63 -97.21 0.44	18.64 17.97 3.73	215
Experiment B FEA_B *% deviation*	286.88 288.07 -0.41	158.22 170.62 -7.27	77.86 76.82 1.36	-63.00 -55.99 12.51	-210.12 -199.15 5.51	-199.46 -188.10 6.04	33.48 33.99 -1.49	415
Experiment C FEA *% deviation*	462.62 430.53 7.45	260.98 255.00 2.34	108.79 114.80 -5.24	-86.91 -83.69 3.86	-307.87 -297.65 3.43	-304.95 -281.13 8.47	51.47 50.80 1.33	620

Experiment D FEA_D *% deviation*	625.66 569.81 9.80	401.06 337.49 18.83	140.58 151.94 -7.48	-114.40 -110.76 3.29	-400.45 -393.93 1.65	-431.33 -372.07 15.93	70.05 67.23 4.20	821
Experiment E FEA_E *% deviation*	787.97 711.60 10.73	550.19 421.47 30.54	185.72 189.75 -2.12	-149.08 -138.32 7.78	-494.18 -491.95 0.45	-605.21 -464.65 30.25	92.60 83.96 10.29	1 026

For the lower loads the correlation between the FEA and strain gauge measurements was found to be mostly within 10%. However, at high loads, for strain gauges 2 and 6, deviations were found to be more than 10%. This is attributed to slight twisting of the implant under these high loads, which would be detected by these two guages due to their positions. Such twisting was indeed observed during experimentation.

Satisfactory correlation was found in this study between FEA results and experimental results from strain gauge measurements.

4. CONCLUSION

The study confirmed that FEA of Ti6Al4V medical implants designed for AM can be validated through using strain gauge measurements. This makes FEA a powerful tool for prediction of stress and strain distributions during the design of complex medical implants as produced through AM.

5. ACKNOWLEDGEMENT

The financial support of the South African Department of Science and Technology through the Collaborative Program in Additive Manufacturing is gratefully acknowledged.

REFERENCES

[1] **ASTM International.** 2013. F2792-12a - Standard Terminology for Additive Manufacturing Technologies. *Rapid Manufacturing Association*, pp.10–12.

[2] **Mellor, S., Hao, L. & Zhang, D.** 2014. Additive manufacturing: A framework for implementation. *International Journal of Production Economics*, 149, pp.194–201.

[3] **Taheri, M. et al.** 2014. Acta Biomaterialia Metals for bone implants . Part 1 . Powder metallurgy and implant rendering. *Acta Biomaterialia*, 10(10), pp.4058–4070.

[4] **Parthasarathy, J., Starly, B. & Raman, S.** 2011. A design for the additive manufacture of functionally graded porous structures with tailored mechanical properties for biomedical applications. *Journal of Manufacturing Processes*, 13(2), pp.160–170.

[5] **Okumura, N. et al.** 2011. Finite element analysis of implant-embedded maxilla model from CT data: comparison with the conventional model. *Journal of prosthodontic research*, 55(1), pp.24–31.

[6] **Lei, T. et al.** 2012. Blast injuries to the human mandible: development of a finite element model and a preliminary finite element analysis. *Injury*, 43(11), pp.1850–5.

[7] **Tang, Z. et al.** 2012. Dynamic simulation and preliminary finite element analysis of gunshot wounds to the human mandible. *Injury*, 43(5), pp.660–5.

[8] **Roylance, D.** 2001. Finite Element Analysis Department of Materials Science and engineering, Massachusetts Institute of Technology Cambridge, MA 02139.

[9] **Correa, S. et al.** 2012. Evaluation of the structural behavior of three and four implant-supported fixed prosthetic restorations by finite element analysis. *Journal of prosthodontic research*, 56(2), pp.110–9.

[10] **Bertol, L.S. et al.** 2010. Medical design: Direct metal laser sintering of Ti-6Al-4V. *Materials and Design*, 31(8), pp.3982–3988.

[11] **Gröning, F. et al**. 2009. Validating a voxel-based finite element model of a human mandible

using digital speckle pattern interferometry. *Journal of biomechanics*, 42(9), pp.1224–9.

[12] **Kromka, M. & Milewski, G.** 2007. Experimental and numerical approach to chosen types of mandibular fractures cured by means of miniplate osteosynthesis. *Acta of Bioengineering and Biomechanics*, 9(2), pp.49–54.

[13] **Gröning, F. et al.** 2012. Improving the validation of finite element models with quantitative full-field strain comparisons. *Journal of biomechanics*, 45(8), pp.1498–506.

[14] **Qin, M. et al.** 2015. Design and optimization of the fixing plate for customized mandible implants. *Journal of Cranio-Maxillofacial Surgery*, 43(7), pp.1296–1302.

[15] **Dongmei, W. et al.** 2005. Design and biomechanical evaluation of a custom lateral mandible titanium prosthesis. *Conference proceedings : Annual International Conference of the IEEE Engineering in Medicine and Biology Society. IEEE Engineering in Medicine and Biology Society. Conference*, 6, pp.6188–6191.

[16] **De Souza Fernandes, A.C. et al**. 2012. Direct and tomographic dimensional analysis of the inter-radicular distance and thickness of the vestibular cortical bone in the parasymphyseal region of adult human mandibles. *British Journal of Oral and Maxillofacial Surgery*, 50(4), pp.350–355.

[17] **Gonzalez, S.M.** 2008. Cortical bone thickness in the maxilla and mandible for mini-implant placement. *ProQuest Dissertations and Theses*, p.76.

[18] **Barão, V. a R. et al.** 2013. Comparison of different designs of implant-retained overdentures and fixed full-arch implant-supported prosthesis on stress distribution in edentulous mandible--a computed tomography-based three-dimensional finite element analysis. *Journal of biomechanics*, 46(7), pp.1312–20.

[19] **Koolstra, J.** 2012. Dynamics of the Human Mastication System. *International and American Associationf or Dental Research*, 13(4), pp.266–376.

[20] **Koolstra, J. & van Eijden, T.M.G**. 2001. A method to predict muscle control in the kinematically and mechanically indeterminate human masticatory system. *Journal of Biomechanics*, 34(9), pp.1179–1188.

[21] **Sato, M. et al.** 2007. Inclination of the occlusal plane is associated with the direction of the masticatory movement path. *European Journal of Orthodontics*, 29(1), pp.21–25.

[22] **Meyer, C. et al.** 1998. Determination of the external forces applied to the mandible during various static chewing tasks. , pp.331–341.

[23] **Hattori, Y. et al**. 2009. Bite forces and their resultants during forceful intercuspal clenching in humans. *Journal of biomechanics*, 42(10), pp.1533–8.

[24] **Anderson, T.L.** 2005. *Fracture Mechanics: Fundamentals and Applications, Third Edition*.

[25] **Arcam.** 2013. Ti6Al4V ELI Titanium Alloy Specification Sheet. , pp.4–6.

[26] **Bradley, J.** 1994. Tech notes. *Whitmire Pest Manage. Q.*, 13(2), p.8.